

Towards rapid analysis with XRF sensor for assessing soil fertility attributes: Effects of dwell time reduction[☆]

Tiago Rodrigues Tavares^{a,*}, José Paulo Molin^b, Elton Eduardo Novais Alves^c, Fábio Luiz Melquiades^d, Hudson Wallace Pereira de Carvalho^a, Abdul Mounem Mouazen^e

^a Laboratory of Nuclear Instrumentation (LIN), Center for Nuclear Energy in Agriculture (CENA), University of São Paulo (USP), Piracicaba, São Paulo 13416000, Brazil

^b Laboratory of Precision Agriculture (LAP), Department of Biosystems Engineering, "Luiz de Queiroz" College of Agriculture (ESALQ), University of São Paulo (USP), Piracicaba, São Paulo 13418900, Brazil

^c Chair of Soil Science, College for Sustainable Agriculture and Environmental Science, Mohammed VI Polytechnic University, BenGuerir 43150, Morocco

^d Laboratory of Applied Nuclear Physics (LFNA), Department of Physics, Londrina State University (UEL), Londrina 86057970, Paraná, Brazil

^e Precision Soil and Crop Engineering Group (Precision SCoRing), Department of Environment, Faculty of Bioscience Engineering, Ghent University, Coupure Links 653, Blok B, 1st Floor, 9000 Gent, Belgium

ARTICLE INFO

Keywords:

Green chemistry
Proximal soil sensing
Soil mobile platforms
Soil health
Site-specific soil management

ABSTRACT

The analysis time used for the diagnosis of soil fertility attributes using portable X-ray fluorescence spectroscopy (XRF) sensors (between 30 and 90 s) is too long for in situ applications. The present study aimed at evaluating the trade-off between dwell time and XRF performance for assessing soil fertility attributes. A total of 102 soil samples acquired in two Brazilian agricultural fields were used, whose spectra were obtained using dwell times of 90, 60, 30, 15, 10, 7, 4, and 2 s to build and validate calibration models for clay, cation exchange capacity, and extractable K and Ca. Results revealed that it is possible to make drastic reductions in the XRF dwell time (from 90 to 2 s), while keeping excellent prediction performance [ratio of performance to interquartile distance (RPIQ) between 3.52 and 8.32] for all the studied attributes. A dwell time of only 2 s performed satisfactorily and is an analysis time suitable for rapid in situ applications. In addition, it was shown that data from spectral databases previously collected that used long dwell times (e.g., 30, 60, 90 s) can be extrapolated to fast applications with shorter dwell times (e.g., 2 and 4 s), once standardization by the detector's live time has been performed. Anyhow, calibrations using a dwell time similar to the one of the validation set tended to show superior results and are therefore recommended. This study addresses the need and provides guidelines for optimizing XRF sensor analysis time for in situ applications in the context of precision agriculture.

1. Introduction

The application of X-ray fluorescence (XRF) sensors for the analysis of soil fertility related attributes has evolved rapidly in recent years (Lima et al., 2019; Nawar et al., 2019; Tavares et al., 2020a). The technique characterizes a wide range of soil elemental composition (e.g., Si, K, Ca, Ti, Fe, Cu, among others), providing complementary information to other proximal soil sensing (PSS) techniques, e.g., apparent electrical conductivity (EC_a) and diffuse reflectance spectroscopy using visible and near-infrared regions (VNIR) (Javadi et al., 2021; Molin and Tavares, 2019; Xu et al., 2019). Today, XRF sensors have become compact and are promising for integration onto mobile platforms and/or

robots (Bosco, 2013).

Portable XRF sensors have been applied manually for in situ analysis for heavy metals determination in soils (Paulette et al., 2015; Weindorf et al., 2013) and geochemical evaluations in soil trenches (Stockmann et al., 2016; Weindorf et al., 2012). Although these in situ analyses have shown good analytical performances, the XRF analysis time (or dwell time) between 30 and 90 s, typically employed, is not compatible with automated in situ analysis for soil fertility mapping (e.g., on-the-go applications), which require faster measurements. For example, both EC_a and VNIR techniques have an almost instantaneous acquisition time (one second per point) that allows on-the-go data acquisitions with high spatial density (e.g., > 250 data points ha⁻¹ at operating speeds of

[☆] The present study is part of the first author's Ph.D thesis presented to the University of São Paulo.

* Corresponding author.

E-mail addresses: tiagosrt@usp.br (T.R. Tavares), HUDSON@cena.usp.br (H.W.P. Carvalho).

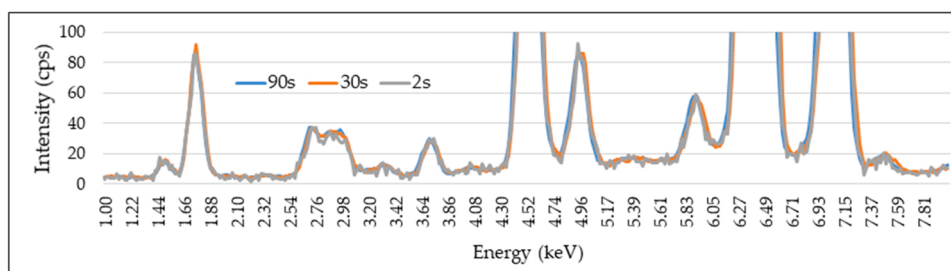


Fig. 1. X-ray fluorescence (XRF) spectra of a soil same sample collected with different scanning times (90, 30 and 2 s), after being standardized by the detector's live time. Counts of photons per second was abbreviated as cps.

around 4 m s^{-1} (Molin and Tavares, 2019). On the other hand, on-the-go application using ion-selective electrodes (ISE) is of similar constrain to that of XRF, since the ISE needs a relatively long dwell time to be in contact with the sample to stabilize its reading (e.g., approximately 10–15 s) (Adamchuk et al., 2007). Anyway, kinematic data acquisitions using ISE systems usually measure about 15–30 data points ha^{-1} (Schirmann et al., 2011), a similar frequency of acquisition should be expected for the XRF if it would be used for on-the-go measurement. Different studies have shown good predictive performances ($0.71 \leq R^2 \leq 0.91$) for key soil fertility attributes (e.g., clay, cation exchange capacity (CEC), base saturation, and exchangeable (ex-) nutrients) using XRF sensors (Andrade et al., 2020; Lima et al., 2019; Tavares et al., 2020b). However, to the best of our knowledge no research has evaluated dwell times smaller than 30 s and neither has searched for an optimal analysis time for rapid and accurate soil attributes predictions.

Reducing the dwell time, increases the noise in XRF spectrum and thus reduces its analytical quality (Weindorf and Chakraborty, 2016). However, despite reducing their accuracy, the spectrum does not have its emission intensity, in counts of photons per second (cps), altered by reducing the dwell time, as can be seen in Fig. 1. The intensity of an XRF spectrum is analyzed in cps when its total count is standardized by the detector's operating time (so-called detector's live time). This standardization should be applied to XRF data because small variations of the detector's live time (e.g., tenths of a second) are commonly observed when analyzing multiple samples (Jenkins, 2012). Errors from this detector variation are avoided by standardizing the XRF spectrum by the live time the detector presented when reading that specific sample. Modeling XRF data (entire spectra or specific emission lines) in cps is a common procedure within the XRF community (Rodrigues et al., 2018; Wolksa, 2005). However, such procedure is not widespread among users from the soil science community, possibly due to the popularization of using pre-programmed measurement packages for XRF soil analysis (Andrade et al., 2021; Lima et al., 2019; Sharma et al., 2015; Silva et al., 2019, 2017), which do not require the user to manipulate the spectral data. Even though, it also does not permit optimizing the instrumental (operational) conditions, such as reducing scanning time (Tavares et al., 2020a).

XRF applications with reduced dwell time are common in analytical chemistry laboratories that are specialized in this technique. The μ -XRF technique (a variant of the XRF technique) uses a micrometric X-ray beam to map elements over the surface of a sample of interest. To cope with the high spatial density of scans (e.g., > 300 spectrum per mm^2), this approach uses a reduced dwell time (e.g., from < 1 –3 s) (Rodrigues et al., 2018). Both the absence of studies in the literature that aim to optimize dwell time for in situ applications, as well as the possibility of analysis with this technique employing dwell times shorter than 5 s, were the motivations to evaluate the performance of the XRF sensor for predicting soil fertility attributes using reduced dwell times. Thus, the following hypothesis (designated as hypothesis 1) was tested in this study: “although reduced dwell times degrade the precision of the XRF prediction due to increasing noise in spectra, it is still possible to

drastically reduce the dwell time while maintaining satisfactory performance for soil fertility prediction”.

Even though in situ applications require reduced analysis time, the model calibration step — that are commonly conducted under laboratory conditions — does not present a time limitation for conducting its data acquisition, which could allow the use of longer dwell times to reduce the problem of increased noise. In this case, models calibrated with longer dwell time would be extrapolated in in situ spectra acquired with short dwell time (e.g., 2 s). Regarding this issue, it is possible to raise the following question “what is the best dwell time for calibrating predictive models that will be extrapolated in rapid XRF predictions during in situ applications (e.g., 2 s)?” To answer this question, this study attempts to address the following hypothesis (designated as hypothesis 2): “calibrations with higher dwell times (e.g., 90, 60, or 30 s) would promote an optimal predictive performance when extrapolating models in spectra acquired using reduced dwell times (e.g., 2 s)”.

This study aimed at evaluating the trade-off between the dwell time reduction and the XRF performance for predicting chemical attributes related to soil fertility (i.e., clay content, CEC, ex-K, and ex-Ca). In addition, this research assessed the performance of models calibrated with data collected at different dwell time scenarios when extrapolated to fast analyzed data (i.e., dwell time of 2). This latter analyses provides initial insights into the feasibility of using pre-existing databases and spectral libraries for the calibration of soil fertility models that will be extrapolated to fast XRF applications. These analyses will encourage further research on the potential of XRF by users in the soil science and precision agriculture community whose research is directed towards rapid analyses, e.g., in situ applications with sensors embedded in agricultural machines and robots for soil mapping.

2. Material and methods

The methodology applied in this study is schematically presented in Fig. 2. The study can be divided into five steps: (i) soil sampling, (ii) soil fertility analyses, (iii) XRF analysis using different dwell times, (iv) characterization of the dwell time effect on the XRF spectra and its predictive performance, and finally (v) definition of an optimized dwell time for model calibration seeking rapid soil fertility analysis.

2.1. Soil samples and fertility analysis

A total of 102 soil samples from Brazilian tropical fields were chosen for this study. These samples belong to the soil sample bank of the Laboratory of Precision Agriculture (LAP – ESALQ/USP), where they are stored after being air-dried and sieved at 2 mm. The chosen soil samples have wide ranges of variability in studied fertility attributes, necessary for the calibration of predictive models. Their texture classes vary among sandy loam, sandy clay loam, and clayey.

The contents of clay, CEC, ex-K, and ex-Ca were determined following the methods described by Van Raij et al. (2001), in which clay content was quantified by the Bouyoucos hydrometer method

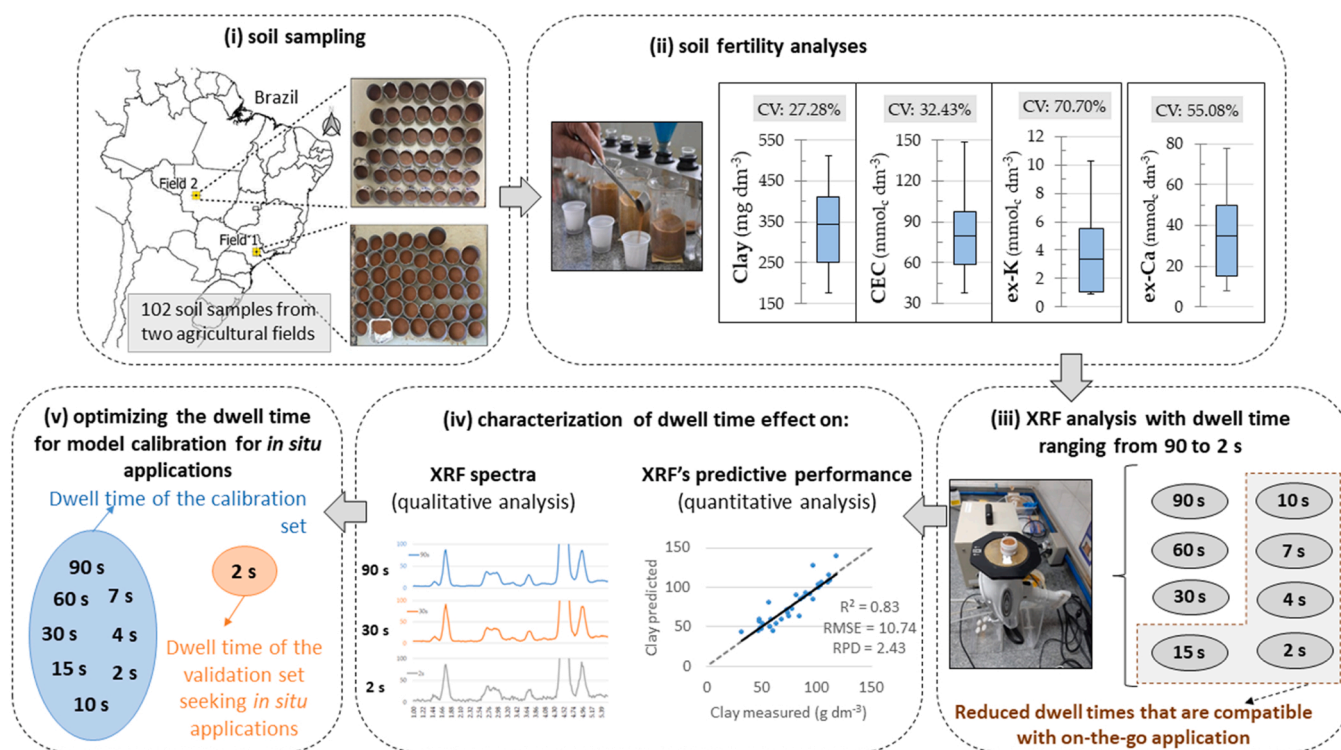


Fig. 2. Framework of the methodology applied for assessing the effect of dwell time reduction in X-ray fluorescence sensor (XRF) for predicting clay, cation exchange capacity (CEC), exchangeable potassium (ex-K), and exchangeable calcium (ex-Ca).

(Bouyoucos, 1951); extractable nutrients via ion exchange resin extraction (van Raij et al., 1986); CEC was calculated as the sum of soil potential acidity ($H + Al$) plus the sum of bases ($ex-Ca + ex-Mg + ex-K$); and $H + Al$ was quantified via pH in the buffer solution method (SMP) (Quaggio et al., 1985). Contents of clay, CEC, ex-K, and ex-Ca were used as reference (Y-variables) for establishing the XRF-spectral modeling.

2.2. XRF measurements and scenarios of dwell time

An amount of about 10 g of each sample was analyzed with a portable XRF sensor. For this, soil samples were placed in a polyethylene cup of 31 mm diameter sealed with a 4- μm thick polypropylene film (model 3520, SPEX, USA). A Tracer III-SD model XRF instrument (Bruker AXS, Madison, EUA) was used for data acquisition. It is a portable device that is equipped with a 4 W Rh X-ray tube and an X-Flash Peltier-cooled Silicon Drift Detector (Bruker AXS, Madison, USA) with 2048 channels. This equipment scans an active area of 10 mm^2 . During data acquisition, the X-ray tube was configured at 35 kV and at 7 μA , while spectra were recorded under atmospheric pressure and without filters, as suggested by Tavares, Mouazen, et al. (2020). These scanning conditions were applied to eight different scenarios of dwell time (90, 60, 30, 15, 10, 7, 4, and 2 s). At each selected time, each sample was scanned in triplicate by slightly moving the position of the sample cup after each replicate. The acquired spectra were normalized by the detector live time, so that net peak area intensity was expressed in counts of photons per second. The replicates of each sample were averaged for further analysis.

2.3. Data analysis

2.3.1. Effects of dwell time reduction on XRF's data

The characterization of XRF data as a function of dwell time reduction was performed by observing the dispersion of signal-to-noise ratio (SNR) in Al, Si, K, Ca, Ti, and Fe $K\alpha$ -lines. These emission lines were

chosen because they emit fluorescence at different energies (1.5, 1.7, 3.3, 3.7, 4.5, and 6.4 keV for Al, Si, K, Ca, Ti, and Fe, respectively), allowing to characterize the effect of dwell time on emission lines that are likely to face different effects.

2.3.2. Effect of dwell time reduction on XRF's prediction performance

The 102 soil samples were split into two subsets, one for calibration (with 68 samples) and the other for validation (with 34 samples) using the Kennard-Stone algorithm (Kennard and Stone, 1969) applied on the measured soil fertility attributes (Y-variables). To evaluate the performance of the prediction models as a function of dwell time reduction, a calibration model obtained with dwell time "X" using the calibration set was validated using its respective validation set obtained with the same dwell time "X". In other words, models using XRF data acquired at 15 s dwell time were validated on XRF data also acquired at 15 s. The intensity (using the net peak area) of nine fluorescence lines ($K\alpha$ emission lines of Al, Si, K, Ca, Ti, Mn, Fe, Ni, and Cu) and two Thomson scattering peaks ($Rh-K\alpha$ and $Rh-L\alpha$) were used as X-variables (Tavares et al., 2020a). Multiple linear regression (MLR) analyses were applied for different dwell times selected. All the calibration and validation steps were performed using the Unscrambler software, version 10.5.1 (Camo AS, Oslo, Norway). Lastly, it is worth emphasizing that all processed spectra (in the different calibration scenarios and also in the validation set) were normalized by the effective dwell time (i.e., detector live time), hence, in all cases the intensity was modelled in counts of photons per second.

The prediction performance was evaluated by means of the root mean square error (RMSE) and the ratio of performance to interquartile distance (RPIQ), the latter was calculated dividing the difference between the third and first quartiles of the laboratory measured soil property by the RMSE of its prediction. Based on the RPIQ values, the prediction quality of developed models were classified into four classes adapted from Nawar and Mouazen (2017): very poor models ($RPIQ \leq 1.40$), fair models ($1.70 \geq RPIQ > 1.40$), good models ($2.00 \geq RPIQ >$

1.70), very good models ($2.5 \geq \text{RPIQ} > 2.0$), and excellent models ($\text{RPIQ} \geq 2.50$). The Tukey test was also applied to the residuals of the predictions performed with each dwell time (having a normal distribution) to compare their performances.

2.3.3. Predictive performance of different dwell times for calibration of models to be extrapolated in applications with short dwell time

In order to find best dwell time for calibrating predictive models that will be extrapolated in rapid XRF predictions during in situ applications (e.g., 2 s), the validation set with spectra acquired with 2 s scanning time were used to extrapolate predictive models calibrated using 90, 60, 30, 15, 10, 7, 4, and 2 s dwell times. The prediction performance of clay, CEC, ex-K, and ex-Ca from the validation set was evaluated. This analysis was conducted because although in situ applications demand a shorter analysis time, the model calibration step can be established under a longer dwell time since it is usually performed under laboratory conditions having less time constraint. The same strategies of data modelling and evaluation of model's performance that were described in the 2.3.2. Section were also applied to the present analysis. Again, the Tukey test was applied to the residuals of the predictions performed with each dwell time to contrast their performances.

3. Results

3.1. Soil fertility attributes

The chosen samples presented high variability of all fertility attributes evaluated, with a coefficient of variation (CV) higher than 27% (Table 1). The Kennard-Stone algorithm allowed to select group of samples with comparable range and SD for both calibration and validation subsets (Table 1), which is essential to avoid undesirable influences on the prediction accuracy that are not related to the XRF sensor (Stenberg et al., 2010).

3.2. Effect of dwell time reduction on XRF data and its predictive performance

The noise was greater for this spectrum collected at a dwell time of 2 s than that of 90 s (Fig. 3A), which reflects the reduction of measurement precision when reducing the dwell time. The reduction of dwell time increased the SNR dispersion for all XRF emission lines but there is no change in the average value (Fig. 3B-G). The standard deviation of fluorescence emission decreases potentially as dwell time

increases (Mondia et al., 2015), this relationship is represented by a power function that was observed in the present data (Fig. A1). This behaviour is influenced by the element concentration in the sample, as well as by the energy of its fluorescence emission (Ravansari et al., 2020), i.e., light elements suffer more interference than heavy ones. Thus different elements show different response to dwell time reduction, as seen in Fig. A1. Among the emission lines evaluated, K presented the lowest SNR (< 4.5) with its CV varying between 7% and 25%. K was the attribute that presented a greater variation of its signal at shorter analysis times, with a CV of the SNR greater than 10% after 30 s. Only the emission lines of Al and Ca showed a CV greater than 10%, which happened only with a dwell time of 2 s. This instability in the sign of K should influence the prediction models that rely on this emission line as the most important predictive variable.

Fig. 4 shows the prediction performance of clay, CEC, ex-K, and ex-Ca models at different dwell times for the same dwell time adopted for the calibration and validation sets. Predictions of clay, CEC, and ex-Ca had a smaller performance variation when reducing the dwell time (with no statistical difference), showing an increase in RMSE ranging from 1.1% to 29.7%. On the other hand, ex-K was the attribute that showed a significant reduction in its prediction performance compared to the best results obtained with 90 s dwell time model (with RMSE increasing between 24.3% and 133.1%). It can be seen that even with the observed RMSE variations, the prediction performances of all fertility attributes remained excellent ($\text{RPIQ} \geq 3.52$) over the entire dwell time reduction (from 90 to 2 s).

The different prediction behavior between clay, CEC, ex-K, and ex-Ca models must be related to the SNR and the dispersion of the models' most important variables. It is important to mention that the main variable for the clay model was the Fe-K α line, for the ex-K model the K-K α , and for the Ca and CEC models the Ca-K α (Table A1). K-K α presented CV values greater than 10% from the 30 s dwell time on, while the K-lines of Al and Ca only presented CV greater values than 10% at the shortest dwell time (i.e., 2 s). In turn, K-lines of Ti, Fe, and Si showed CV $< 4.7\%$ in all dwell times (Fig. 3). Notwithstanding, ex-K prediction still showed an excellent performance ($\text{RPIQ} = 3.57$) with points closely distributed around the 1:1 line (Fig. A2), even in the most reduced dwell time scenario of 2 s

3.3. Effect of model calibration using data with different dwell times

Fig. 5 shows the performance of models calibrated using XRF data (of the calibration set) acquired at different dwell times (90, 60, 30, 15, 10,

Table 1
Descriptive statistics of soil fertility attributes for the calibration and validation dataset.

	Clay g dm ^{-c}	CEC ^a	ex-K ^b	ex-Ca ^b mmolc dm ^{-c}
Calibration set (n = 68)				
Min	175.00	37.50	0.90	8.00
Mean	352.00	81.75	3.41	35.69
Max	511.00	148.90	10.30	78.00
SD ^c	95.21	25.86	2.48	19.08
CV ^d (%)	27.05	31.63	72.73	53.44
Validation set (n = 34)				
Min	175.00	42.50	0.90	8.00
Mean	332.12	76.50	3.36	33.32
Max	463.00	138.40	7.90	75.00
SD	92.03	26.14	2.26	19.71
CV (%)	27.71	34.17	67.39	59.16

^a Cation exchange capacity

^b exchangeable (ex-) nutrients

^c standart deviation

^d coefficient of variation.

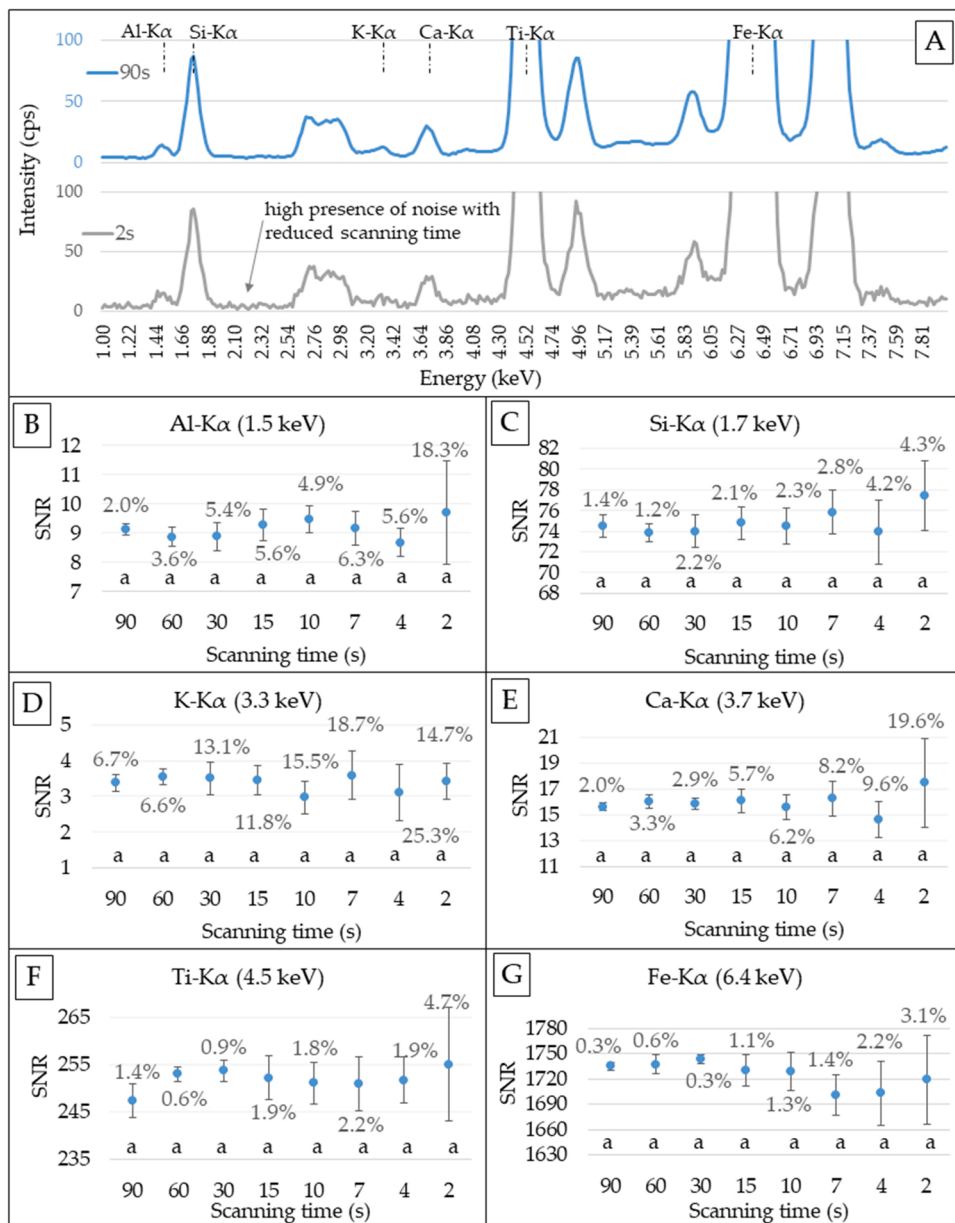


Fig. 3. Effect of dwell time reduction on XRF spectra (A). Signal-to-noise ratio (SNR) is shown for the K-lines of Al (B), Si (C), K (D), Ca (E), Ti (F), and Fe (G) obtained at different dwell times (2, 4, 7, 10, 15, 30, 60, and 90 s). The bars represent the standard deviation and the values in percentage represent the coefficient of variation of five XRF measurements (replicates) performed on the same soil sample after moving the sample cup position. Counts of photons per second was abbreviated as cps. There were no statistical difference between the means at $P < 0.05$ (Tukey test).

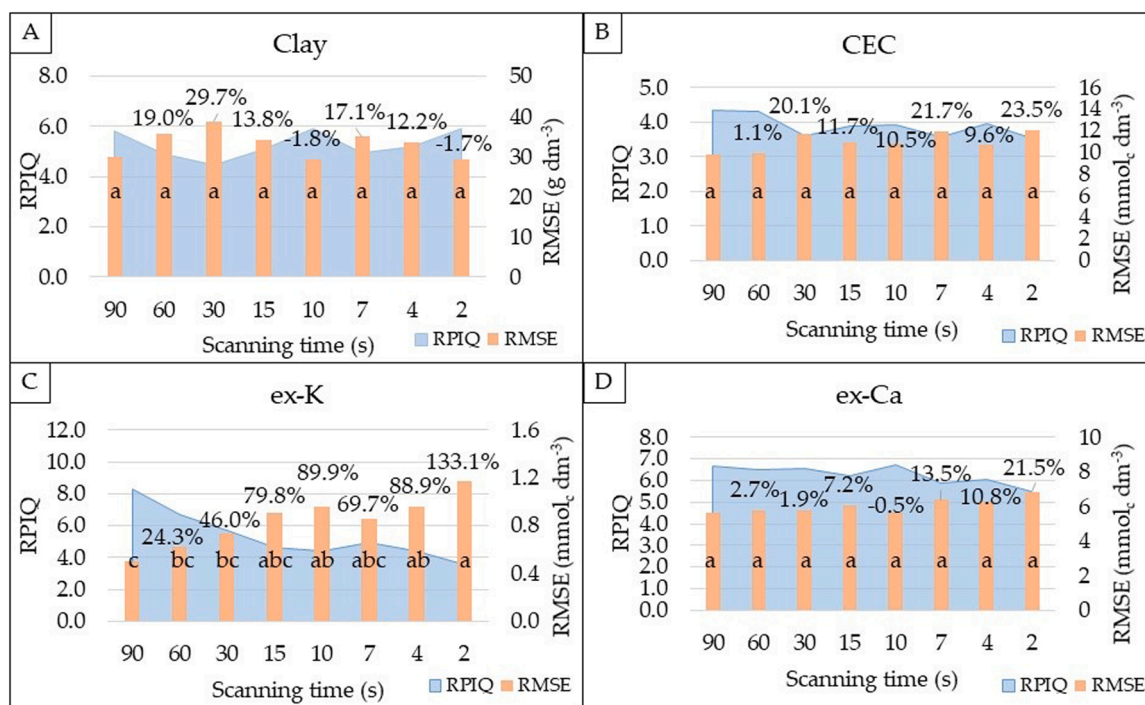


Fig. 4. Effect of dwell time on X-ray fluorescence (XRF) sensor performance for clay (A), cation exchange capacity (CEC) (B), exchangeable (ex-) K (C) and ex-Ca (D) prediction (using the validation set, $n = 34$) for the same dwell time of both the calibration and validation set. The performance was evaluated via the ratio of performance to interquartile distance (RPIQ) and root-mean-square error (RMSE). The percentage values represent the variation of RMSE in relation to the performance obtained with 90 s dwell time. The calibration and validation set were obtained with the same dwell time as detailed in 2.3.2. Section. The most important variables and the scatter plots of the models calibrated at 90 and 2 s are shown in Table A1 and Fig. A2 (Appendix Section), respectively. Different letters indicate a significant difference at $P < 0.05$ (Tukey test).

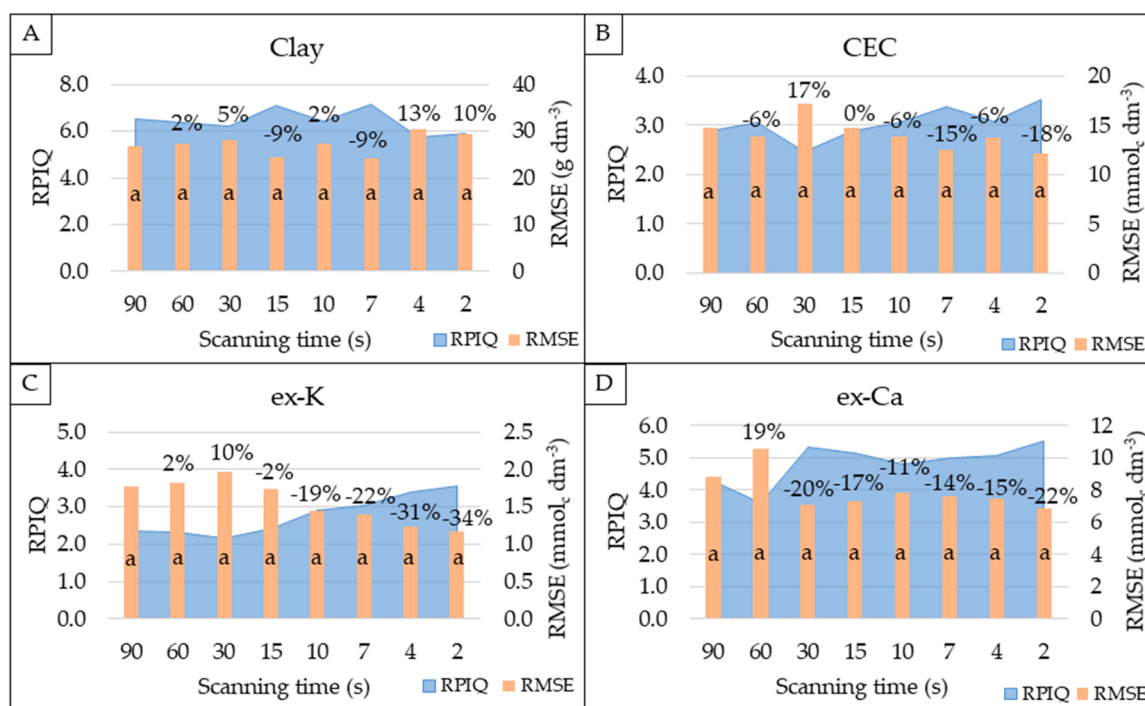


Fig. 5. X-ray fluorescence (XRF) performance for clay (A), cation exchange capacity (CEC) (B), exchangeable (ex-) K (C) and ex-Ca (D) prediction, using different dwell times (90, 60, 30, 15, 10, 7, 4, and 2 s) in model calibration. The results represent the extrapolation of these different calibration scenarios in the validation set ($n = 34$) that was analyzed with 2 s of dwell time. The performance was evaluated via the ratio of performance to interquartile distance (RPIQ) and root-mean-square error (RMSE). The percentage values represent the variation of RMSE in relation to the performance obtained with 90 s dwell time. Similar letters indicate no statistical difference at $P < 0.05$ (Tukey test).

7, 4, and 2 s) when they were extrapolated to data (of the validation set) acquired at 2 s of dwell time, i.e., a dwell time simulating what would be done in rapid applications. For all attributes, Tukey's test indicated no statistical difference in predictive performance when using calibration sets with different dwell times. Despite the absence of statistical difference, it was observed that the ex-K models tends to perform better as the dwell time of the calibration set comes closer to the dwell time of the validation set. For example, the prediction of ex-K using the calibration set at 7, 4, and 2 s has 22%, 31%, and 34% lower errors than when using the models with 90 s dwell time. This behavior was not observed for clay, whose prediction showed stable trend across the different dwell times adopted in the calibration set (with RMSE ranging from 26.70 g dm⁻³ at 90 s to 29.4 g dm⁻³ at 2 s, representing a variation of 10%). Although the predictions of CEC and ex-Ca showed the best performance when calibrated and validated with the same dwell time of 2 s (with RPIQ values of 3.52 and 5.50, respectively), this tendency, i.e., improve the predictive performance as the dwell time of the calibration set approaches that of the validation set, cannot be clearly observed for these attributes, as can be done for the ex-K.

The different prediction behavior among the models of clay, CEC, ex-K, and ex-Ca must be related to the SNR and the dispersion of the models' most important variables (Table A1). Elements with a low SNR emission line have a lower analytical precision, since external factors (e.g., physical and chemical matrix effect) will affect their intensity to a greater extent compared to a high SNR line (An et al., 2021) (this is further discussed in Section 4). The Fe-K α emission line, that is the main variable contributing to clay model (Table A1), had SNR larger than 1500 and CV always smaller than 4% (Fig. 3). In turn, CEC and ex-Ca models rely mainly on Ca-K α emission line, whose SNR ranged between 13 and 21 and CV from 2.0% to 19.6% (with CV > 10% only for 2 s dwell time) (Fig. 3). Finally, the K-K α emission line, main variable of ex-K models, had the lowest SNR (< 5) and CV variation greater than 10% from 30 to 2 s of dwell time, which represents a larger variation than that observed for the other emission lines (Fig. 3).

In summary, the results showed that there was no significant difference for clay, CEC, ex-Ca, and ex-K models, calibrated with 90, 60, 30, 15, 10, 7, 4 and 2 s data to predict these attributes on data acquired at 2 s of dwell time. Nevertheless, the CEC, ex-Ca, and ex-K models, especially the latter, showed a tendency to perform better as the dwell time of the calibration set comes closer to the dwell time of the validation set. Finally, the same trend of prediction described above was also verified when the models were applied to an independent validation set collected with 4 s dwell time (Fig. A3, Appendix Section).

4. Discussion

The results evidenced that XRF readings lose precision as its dwell time is reduced, which is explained by the increased noise at low dwell times. This behaviour occurs mainly for light elements that are close to the detection limit (Ravansari et al., 2020), as observed for K, which showed a greater variation in its fluorescence emission and a lower SNR (< 5). Obtaining stable measurements with reduced analysis time is also related to the level of technology of the equipment's detector. New generations of detectors have delivered lower noise at shorter analysis times, and these advances expand the applications with XRF sensors (Bosco, 2013), such as the one discussed in this paper.

Even though readings taken with a short analysis time reduce the precision compared to longer times, the XRF accuracy for predicting fertility attributes does not degrade expressively. This trend was observed even for the prediction of ex-K, whose models were based on the K emission line, but achieved excellent prediction performances for all evaluated dwell times, even for the most reduced dwell time scenario of 2 s (RPIQ = 3.57). Therefore, it is possible to drastically reduce the sensor's dwell time (e.g., from 90 to 2 s), while maintaining satisfactory predictive performances (RPIQ \geq 3.52). Thus, the authors accept the first hypothesis of this study that although low dwell times degrade the

XRF prediction accuracy, it is still possible to drastically reduce the dwell time while maintaining satisfactory performance for soil fertility prediction (namely, clay, CEC, ex-K, and ex-Ca). No study in the literature has evaluated the prediction performance of soil fertility attributes using scanning time as short as that presented in the current research. Evaluating dwell time of 60, 120 and 180 s for P prediction in leaf samples, Sapkota et al. (2019) observed that the time of analysis had no significant influence on the performance of the models, having R² ranging from 0.84 to 0.88. In tropical soils, some authors have reported no significant differences in attribute predictions made with dwell times of 30 and 60 s (Silva et al., 2019, 2018). Although the aforementioned studies did not evaluate drastic reductions in analysis time, they don't notice any performance loss in XRF prediction when using contrasting dwell times, which corroborates the results observed in the present study.

The accuracy to measure a given element with XRF set at short dwell times is linked to intrinsic aspects related to its fluorescence emission line (i.e., lighter elements that have lower fluorescence emission and lower energies are more affected), as well as to the concentration of this element in the sample (Ravansari et al., 2020; Silva et al., 2021). That is, light elements with low content in the analyzed soil sample (i.e., close to their limit of detection and with a lower SNR) are more affected by the loss of accuracy when reducing the scanning time. This behavior occurs because the fluorescence emission of these elements have a lower SNR and, therefore, any external interference (i.e., physical and chemical matrix effects) will have a greater effect on its intensity (An et al., 2021; Ernst et al., 2014). In this study, the lower SNR of the K emission line (< 10) caused a higher interference in the ex-K prediction model when changing the dwell time. Similarly, the clay, CEC, and ex-Ca models that were related to emission lines with higher SNR (i.e., Fe-K α for clay models and Ca-K α for CEC and ex-Ca models), had a higher stability when changing the dwell time. In addition, it is worth commenting that SNR values lower than 10 are considered critical and lead to poor modelling results (Danzer and Currie, 1998), indicating that the element present concentrations are closer to the limit of detection for the instrumental conditions adopted. Optimizing the instrumental conditions to increase the K-K α SNR may be a strategy to be considered in the future to improve the performance of ex-K prediction under low dwell time conditions.

Regarding the effect of dwell time for model calibration, the results showed that, once the data are standardized by the detector's live time, the model can be calibrated with dwell times ranging from 90 to 2 s and successfully extrapolated on data collected with dwell times of 4 and 2 s (Fig. 5 and Fig. A3). So, spectral library data previously obtained with longer dwell times (e.g., 30, 60, 90 s) can be used for XRF applications with rapid measurements such that the predictive performance will not significantly deteriorate due to different dwell times. Despite the absence of a significant difference, models based on emission lines with lower SNR (especially ex-K models in this study) showed a tendency to perform better as the dwell time of the calibration set comes closer to the dwell time of the validation set. In light of these results, it is suggested that the calibration step should be performed with spectral data acquired with the same dwell time as the one intended to be implemented in the field. This can be suggested, because the prediction accuracy using longer dwell times did not lead to a better performance of predictions (Fig. 5 and Fig. A3), as raised by the second hypothesis of this study; hence, it was rejected.

The findings show that XRF may be suitable for accurate in situ rapid analysis of key soil fertility attributes. This knowledge is not widespread among XRF users as it is quite common to use pre-programmed measurement packages (Andrade et al., 2020; Horta et al., 2015; Lima et al., 2019; Nawar et al., 2019; O'Rourke et al., 2016), which are factory calibrations (for determining total elemental concentration), associated with a pre-established dwell time, generally between 30 and 90 s (Weindorf and Chakraborty, 2016). Based on the results presented in this study, XRF users within the precision agriculture and soil science

communities should be encouraged to use open systems that allow the optimization of dwell time, since this will enable the expansion of XRF applications in such context.

Unlike laboratory measurements that are mainly conducted on dried and sieved samples, in field applications fresh unprocessed soils are measured, which means that external factors, such as soil moisture and roughness, will influence sensors' output (Horta et al., 2015; Mouazen and Al-Asadi, 2018; Nawar et al., 2020). To support future in situ applications of XRF sensors for soil mapping, further studies should evaluate the combination of rapid XRF analysis on fresh (wet) samples, representing the soil conditions at the time of data acquisition directly in the field. Evaluation of similar solutions to those adopted to mitigate performance loss on the near infrared and mid infrared spectroscopy sensors (Minasny et al., 2011; Nawar et al., 2020; Roger et al., 2003) due to external factors, such as the moisture content, may be a next step to consider for XRF analysis.

5. Conclusions

The results showed that reducing the dwell time of X-ray fluorescence (XRF) analysis decreases the precision of its data. In spite of that, it was possible to achieve excellent prediction performance [ratio of performance to interquartile distance (RPIQ) ≥ 3.52] of soil fertility attributes (clay, cation exchange capacity, and exchangeable K and Ca) even after applying drastic reductions of XRF's dwell time (from 90 to 2 s).

In addition, this study also evaluated and suggested an optimized dwell time for model calibration (which is generally conducted in the laboratory without time restriction) seeking rapid soil fertility analysis. The results suggested that the best calibration models are those conducted with the same dwell time as the validation set (e.g., calibrated and validated using spectra acquired at 2 s of dwell time), refuting the idea that a longer dwell time should guarantee a more accurate data for model calibration. In any case, using longer dwell times for model calibration did not lead to statistically significant differences in the validation results. Therefore, this research also indicates that previously existing spectral libraries can be used to calibrate models that will be extrapolated on XRF data obtained from rapid measurements without significant losses in performance.

These results allow bringing XRF closer to *in site* soil fertility mapping in the precision agriculture context. Researchers are encouraged to combine reduced dwell times with the removal of other external factors affecting in in situ data (e.g., soil moisture, soil roughness, etc) to optimize the use of XRF directly in the field for soil fertility prediction.

Declaration of Competing Interest

The authors declare that they have no known competing financial

Table A1

Importance of X-ray fluorescence (XRF) variables for the prediction of clay, cation exchange capacity (CEC), (ex-) K and Ca, using the dwell times of 90 and 2 s. The values presented correspond to the t-value for each standardized coefficient obtained in the fitted regressions. The emboldened values indicate a significant t-values at the probability level of 0.05; significant values were presented on grayscale, with the most important variables having the darkest color and vice versa.

	Dwell time (s)	Al-K α	Si-K α	K-K α	Ca-K α	Ti-K α	Mn-K α	Fe-K α	Ni-K α	Cu-K α	Rh-K α	Rh-L α
clay	90	-0.61	-1.35	0.05	-0.79	-3.48	-0.31	6.56	0.11	-1.69	-1.66	0.92
	2	-0.92	-2.16	-0.40	-0.80	-2.29	-0.35	7.13	-1.24	-1.73	0.25	-1.38
CEC	90	-1.67	0.17	1.72	4.67	3.20	-2.84	-1.27	-0.61	1.38	-0.67	0.86
	2	-1.16	-0.41	1.08	4.00	3.45	-2.42	-1.06	-1.12	0.46	0.21	1.63
ex-K	90	-1.92	0.35	16.18	-4.41	-0.16	-2.00	0.33	-1.36	-0.90	-1.23	-1.39
	2	-2.34	-1.34	7.14	-2.21	0.23	1.29	-0.58	0.59	-1.30	-1.37	-1.89
ex-Ca	90	-3.33	2.29	1.78	8.53	1.46	-3.65	1.92	-0.39	0.37	0.08	1.26
	2	-3.26	2.15	0.87	8.93	2.43	-3.34	2.97	0.12	-0.93	-0.57	-0.02

interests or personal relationships that could have appeared to influence the work reported in this paper.

Data availability

Data will be made available on request.

Acknowledgments

Tiago R. Tavares was funded by São Paulo Research Foundation (FAPESP), grant number 2020/16670-9. We also thank the research productivity fellowship from the Brazilian National Council for Scientific and Technological Development (CNPq) (grant numbers 306185/2020-2 and 310446/2020-1). XRF facilities were funded by FAPESP, grant number 2015-19121-8, and "Financiadora de Estudos e Projetos" (FINEP) project "Core Facility de suportes às pesquisas em Nutrologia e Segurança Alimentar na USP", grant number 01.12.0535.0. Authors also acknowledge the financial support received from the Research Foundation-Flanders (FWO) for Odysseus I SiTeMan Project (no. G0F9216N).

Appendix

Fig. A1 shows the exponential behavior of the standard deviation as a function of dwell time for the K-lines of Al, Si, K, and Ca. Table A1 shows the importance of the spectral variables used for the model calibration for predicting clay, CEC, ex-K, and ex-Ca, using the dwell times of 90 and 2 s

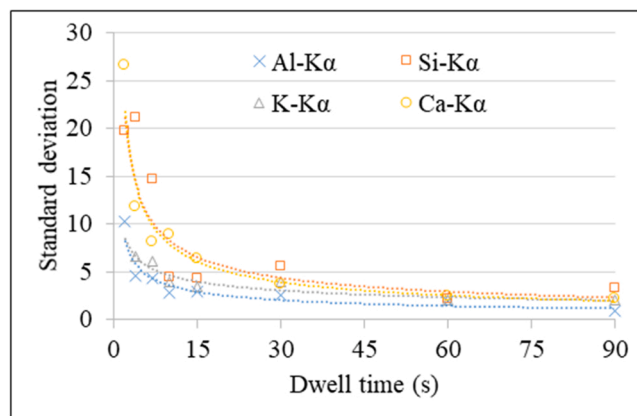


Fig. A1. Scatter plots of dwell time versus standard deviation of Al-, Si-, K-, and Ca-K lines obtained from five XRF measurements performed on the same soil sample after moving the sample cup position.

Fig. A2 shows the scatter plots of predicted versus measured clay, CEC, ex-K, and ex-Ca, for the validation set (n = 34) of models that were calibrated and validated using dwell times of 90 and 2 s. Finally,

the Fig. A3 shows the results for the dwell time optimization for calibrating models seeking in situ applications, a similar analysis to the one detailed in Section 2.3.3., but now replicating all the evaluated dwell

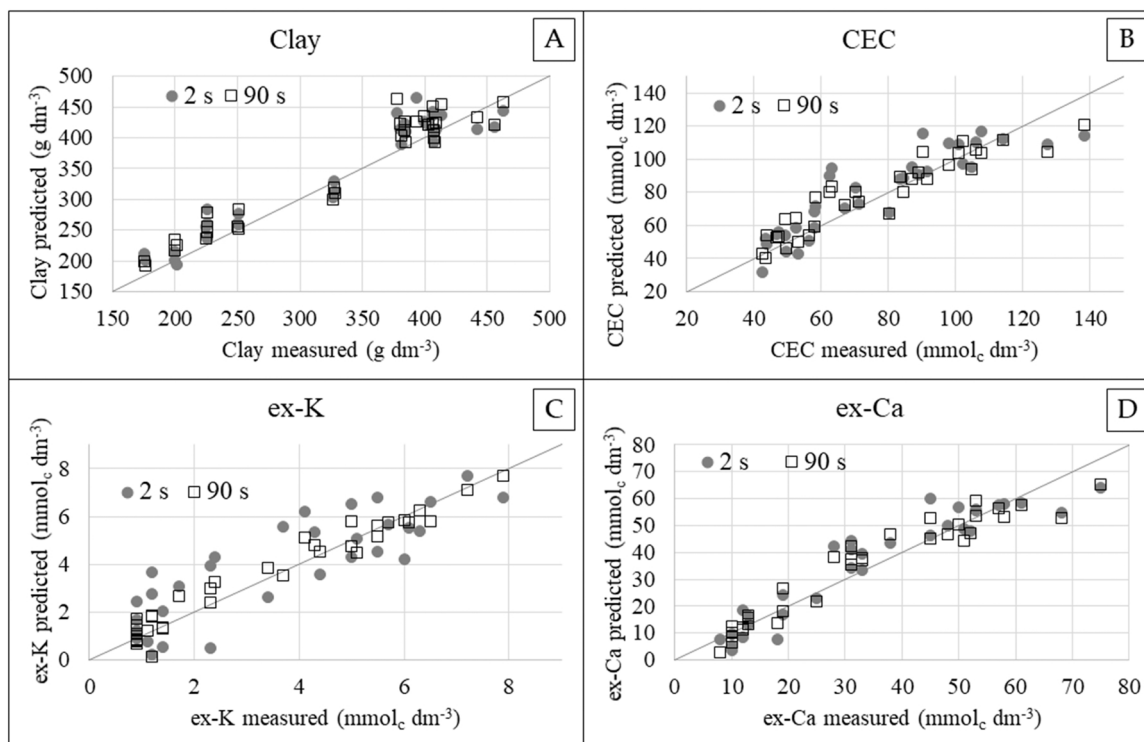


Fig. A2. Scatter plots of predicted versus measured clay (A), cation exchange capacity (CEC) (B), exchangeable (ex-) K (C) and Ca (D) using dwell times of 90 and 2 s.

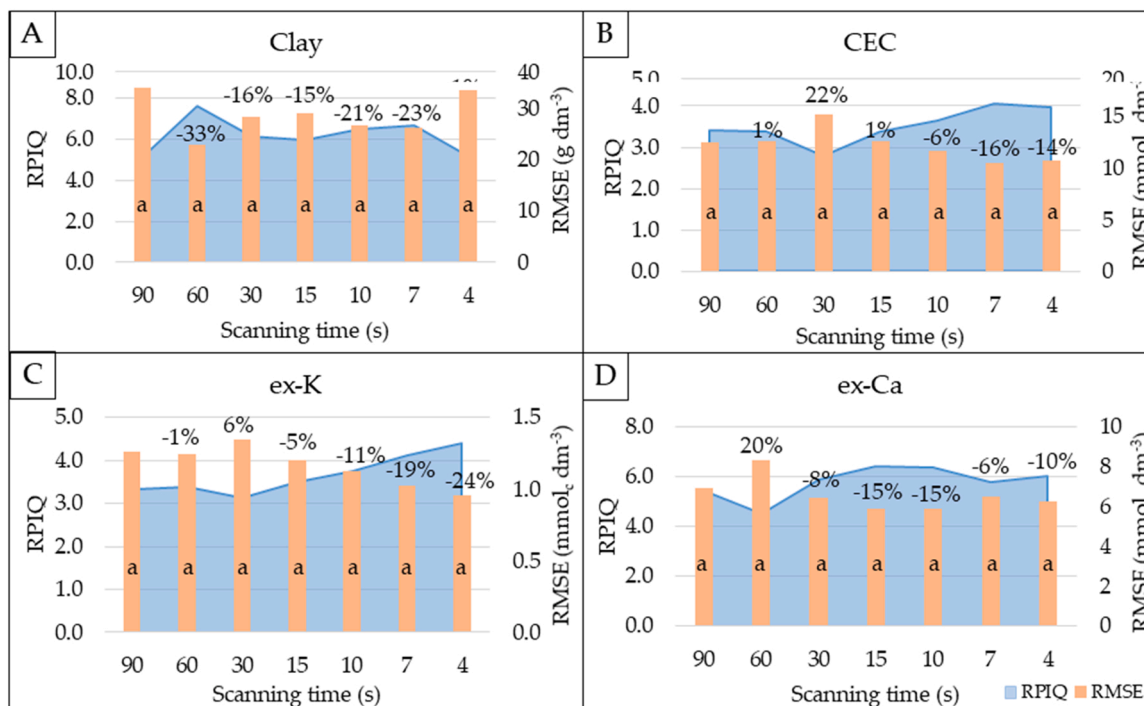


Fig. A3. Calibration performance using different dwell times (90, 60, 30, 15, 10, 7, and 4 s) for the calibration of models for the prediction of clay (A), cation exchange capacity (CEC) (B), exchangeable (ex-) K (C) and Ca (D). The results represent the validation of these different calibration scenarios when replicated on the validation set (n = 34) scanned with 4 s of dwell time. The performance was evaluated via the ratio of performance to interquartile distance (RPIQ) and root-mean-square error (RMSE). The percentage values represent the variation of RMSE in relation to the performance obtained with 90 s dwell time. Similar letters indicate no statistical difference at P < 0.05 (Tukey test).

times (90, 60, 30, 15, 10, 7, 4, and 2 s) in spectra acquired with 4 s of dwell time. The results (Fig. A3) show that the behavior was the same as that observed for 2 s (described in Section 3.3.).

References

- Adamchuk, V.I., Lund, E.D., Reed, T.M., Ferguson, R.B., 2007. Evaluation of an on-the-go technology for soil pH mapping. *Precis. Agric.* 8, 139–149. <https://doi.org/10.1007/s11119-007-9034-0>.
- An, S., Reza, S., Norlin, B., Fröjdch, C., Thungström, G., 2021. Signal-to-noise ratio optimization in X-ray fluorescence spectrometry for chromium contamination analysis. *Talanta* 230, 122236. <https://doi.org/10.1016/j.talanta.2021.122236>.
- Andrade, R., Faria, W.M., Silva, S.H.G., Chakraborty, S., Weindorf, D.C., Mesquita, L.F., Guilherme, L.R.G., Curi, N., 2020. Prediction of soil fertility via portable X-ray fluorescence (pXRF) spectrometry and soil texture in the Brazilian Coastal Plains. *Geoderma* 357, 113960. <https://doi.org/10.1016/j.geoderma.2019.113960>.
- Andrade, R., Silva, S.H.G., Weindorf, D.C., Chakraborty, S., Faria, W.M., Guilherme, L.R.G., Curi, N., 2021. Micronutrients prediction via pXRF spectrometry in Brazil: Influence of weathering degree. *Geoderma Reg.* 27, e00431 <https://doi.org/10.1016/j.geodrs.2021.e00431>.
- Bosco, G.L., 2013. Development and application of portable, hand-held X-ray fluorescence spectrometers. *TrAC Trends Anal. Chem.* 45, 121–134. <https://doi.org/10.1016/j.trac.2013.01.006>.
- Bouyoucos, G.J., 1951. A Recalibration of the Hydrometer Method for Making Mechanical Analysis of Soils 1. *Agron. J.* 43, 434–438. <https://doi.org/10.2134/agronj1951.00021962004300090005x>.
- Danzer, K., Currie, L.A., 1998. Guidelines for calibration in analytical chemistry. Part I. Fundamentals and single component calibration (IUPAC Recommendations 1998). *Pure Appl. Chem.* 70, 993–1014. <https://doi.org/10.1351/pac199870040993>.
- Ernst, T., Berman, T., Buscaglia, J., Eckert-Lumsdon, T., Hanlon, C., Olsson, K., Palenik, C., Ryland, S., Trejos, T., Valadez, M., Almirall, J.R., 2014. Signal-to-noise ratios in forensic glass analysis by micro X-ray fluorescence spectrometry. *X-Ray Spectrom.* 43, 13–21. <https://doi.org/10.1002/xrs.2437>.
- Horta, A., Malone, B., Stockmann, U., Minasny, B., Bishop, T.F.A., McBratney, A.B., Pallasser, R., Pozza, L., 2015. Potential of integrated field spectroscopy and spatial analysis for enhanced assessment of soil contamination: A prospective review. *Geoderma* 241–242, 180–209. <https://doi.org/10.1016/j.geoderma.2014.11.024>.
- Javadi, S.H., Munnaf, M.A., Mouazen, A.M., 2021. Fusion of Vis-NIR and XRF spectra for estimation of key soil attributes. *Geoderma* 385, 114851. <https://doi.org/10.1016/j.geoderma.2020.114851>.
- Jenkins, R., 2012. *X-Ray Fluorescence Spectrometry*. John Wiley & Sons, Hoboken, NJ, USA.
- Kennard, R.W., Stone, L.A., 1969. Computer aided design of experiments. *Technometrics* 11, 137–148. <https://doi.org/10.1080/00401706.1969.10490666>.
- Lima, T.M., de, Weindorf, D.C., Curi, N., Guilherme, L.R.G.G., Lana, R.M.Q.Q., Ribeiro, B. T., 2019. Elemental analysis of Cerrado agricultural soils via portable X-ray fluorescence spectrometry: Inferences for soil fertility assessment. *Geoderma* 353, 264–272. <https://doi.org/10.1016/j.geoderma.2019.06.045>.
- Minasny, B., McBratney, A.B., Bellon-Maurel, V., Roger, J.-M., Gobrecht, A., Ferrand, L., Joalland, S., 2011. Removing the effect of soil moisture from NIR diffuse reflectance spectra for the prediction of soil organic carbon. *Geoderma* 167–168, 118–124. <https://doi.org/10.1016/j.geoderma.2011.09.008>.
- Molin, J.P., Tavares, T.R., 2019. Sensor systems for mapping soil fertility attributes: challenges, advances, and perspectives in Brazilian tropical soils. *Eng. Agric.* 39, 126–147. <https://doi.org/10.1590/1809-4430-eng.agric.v39nep126-147/2019>.
- Mondia, J.P., Goh, F., Bryngelson, P.A., MacPhee, J.M., Ali, A.S., Weiskopf, A., Lanam, M., 2015. Using X-ray fluorescence to measure inorganics in biopharmaceutical raw materials. *Anal. Methods* 7, 3545–3550. <https://doi.org/10.1039/C4AY02936D>.
- Mouazen, A.M., Al-Asadi, R.A., 2018. Influence of soil moisture content on assessment of bulk density with combined frequency domain reflectometry and visible and near infrared spectroscopy under semi field conditions. *Soil Tillage Res* 176, 95–103. <https://doi.org/10.1016/j.still.2017.11.002>.
- Nawar, S., Mouazen, A.M., 2017. Predictive performance of mobile vis-near infrared spectroscopy for key soil properties at different geographical scales by using spiking and data mining techniques. *CATENA* 151, 118–129. <https://doi.org/10.1016/j.catena.2016.12.014>.
- Nawar, S., Delbecq, N., Declercq, Y., De Smedt, P., Finke, P., Verdoodt, A., Van Meirvenne, M., Mouazen, A.M., 2019. Can spectral analyses improve measurement of key soil fertility parameters with X-ray fluorescence spectrometry? *Geoderma* 350, 29–39. <https://doi.org/10.1016/j.geoderma.2019.05.002>.
- Nawar, S., Abdul Munnaf, M., Mouazen, A.M., 2020. Machine Learning Based On-Line Prediction of Soil Organic Carbon after Removal of Soil Moisture Effect. *Remote Sens* 12, 1308. <https://doi.org/10.3390/rs12081308>.
- O'Rourke, S.M., Stockmann, U., Holden, N.M., McBratney, A.B., Minasny, B., 2016. An assessment of model averaging to improve predictive power of portable vis-NIR and XRF for the determination of agronomic soil properties. *Geoderma* 279, 31–44. <https://doi.org/10.1016/j.geoderma.2016.05.005>.
- Paulette, L., Man, T., Weindorf, D.C., Person, T., 2015. Rapid assessment of soil and contaminant variability via portable x-ray fluorescence spectroscopy: Copsa Mică, Romania. *Geoderma* 243–244, 130–140. <https://doi.org/10.1016/j.geoderma.2014.12.025>.
- Quaggio, J.A., van Raij, B., Malavolta, E., 1985. Alternative use of the SMP-buffer solution to determine lime requirement of soils. *Commun. Soil Sci. Plant Anal.* 16, 245–260. <https://doi.org/10.1080/00103628509367600>.
- van Raij, B., Quaggio, J.A., da Silva, N.M., 1986. Extraction of phosphorus, potassium, calcium, and magnesium from soils by an ion-exchange resin procedure. *Commun. Soil Sci. Plant Anal.* 17, 547–566. <https://doi.org/10.1080/00103628609367733>.
- Ravansari, R., Wilson, S.C., Tighe, M., 2020. Portable X-ray fluorescence for environmental assessment of soils: Not just a point and shoot method. *Environ. Int.* 134, 105250. <https://doi.org/10.1016/j.envint.2019.105250>.
- Rodrigues, E.S., Gomes, M.H.F., Duran, N.M., Cassanji, J.G.B., da Cruz, T.N.M., Sant'Anna Neto, A., Savassa, S.M., de Almeida, E., Carvalho, H.W.P., 2018. Laboratory microprobe X-ray fluorescence in plant science: emerging applications and case studies. *Front. Plant Sci.* 9, 1588. <https://doi.org/10.3389/fpls.2018.01588>.
- Roger, J.-M., Chauchard, F., Bellon-Maurel, V., 2003. EPO-PLS external parameter orthogonalisation of PLS application to temperature-independent measurement of sugar content of intact fruits. *Chemom. Intell. Lab. Syst. Syst.* 66, 191–204. [https://doi.org/10.1016/S0169-7439\(03\)00051-0](https://doi.org/10.1016/S0169-7439(03)00051-0).
- Sapkota, Y., McDonald, L.M., Griggs, T.C., Basden, T.J., Drake, B.L., 2019. Portable X-ray fluorescence spectroscopy for rapid and cost-effective determination of elemental composition of ground forage. *Front. Plant Sci.* 10. <https://doi.org/10.3389/fpls.2019.00317>.
- Schirmann, M., Gebbers, R., Kramer, E., Seidel, J., 2011. Soil pH Mapping with an On-The-Go Sensor. *Sensors* 11, 573–598. <https://doi.org/10.3390/s110100573>.
- Sharma, A., Weindorf, D.C., Wang, D., Chakraborty, S., 2015. Characterizing soils via portable X-ray fluorescence spectrometer: 4. Cation exchange capacity (CEC). In: *Geoderma*, 239–240, pp. 130–134. <https://doi.org/10.1016/j.geoderma.2014.10.001>.
- Silva, E.A., Weindorf, D.C., Silva, S.H.G., Ribeiro, B.T., Poggere, G.C., Carvalho, T.S., Gonçalves, M.G.M., Guilherme, L.R.G., Curi, N., 2019. Advances in Tropical Soil Characterization via Portable X-Ray Fluorescence Spectrometry. *Pedosphere* 29, 468–482. [https://doi.org/10.1016/S1002-0160\(19\)60815-5](https://doi.org/10.1016/S1002-0160(19)60815-5).
- Silva, S.H.G., Teixeira, A.F., dos, S., Menezes, M.D., de, Guilherme, L.R.G., Moreira, F.M., de, S., Curi, N., Silva, S.H.G., Teixeira, A.F., dos, S., Menezes, M.D., de, Guilherme, L.R.G., Moreira, F.M., de, S., Curi, N., 2017. Multiple linear regression and random forest to predict and map soil properties using data from portable X-ray fluorescence spectrometer (pXRF). *Ciência e Agrotecnologia* 41, 648–664. <https://doi.org/10.1590/1413-7054201741610317>.
- Silva, S.H.G., Silva, E.A., Poggere, G.C., Guilherme, L.R.G., Curi, N., 2018. Tropical soils characterization at low cost and time using portable X-ray fluorescence spectrometer (pXRF): Effects of different sample preparation methods. *Ciência e Agrotecnologia* 42, 80–92. <https://doi.org/10.1590/1413-70542018421009117>.
- Silva, S.H.G., Ribeiro, B.T., Guerra, M.B.B., de, Carvalho, H.W.P., Lopes, G., Carvalho, G. S., Guilherme, L.R.G., Resende, M., Mancini, M., Curi, N., Rafael, R.B.A., Cardelli, V., Cocco, S., Corti, G., Chakraborty, S., Li, B., Weindorf, D.C., 2021. pXRF in tropical soils: methodology, applications, achievements and challenges. *Adv. Agron.* 167, 1–62. <https://doi.org/10.1016/bs.agron.2020.12.001>.
- Stenberg, B., Viscarra Rossel, R.A., Mouazen, A.M., Wetterlind, J., 2010. Visible and near infrared spectroscopy in soil science. *Adv. Agron.* 107, 163–215. [https://doi.org/10.1016/S0065-2113\(10\)07005-7](https://doi.org/10.1016/S0065-2113(10)07005-7).
- Stockmann, U., Cattle, S.R., Minasny, B., McBratney, A.B., 2016. Utilizing portable X-ray fluorescence spectrometry for in-field investigation of pedogenesis. *CATENA* 139, 220–231. <https://doi.org/10.1016/j.catena.2016.01.007>.
- Tavares, T.R., Molin, J.P., Nunes, L.C., Alves, E.E.N., Melquiades, F.L., de Carvalho, H.W.P., Mouazen, A.M., Carvalho, H.W.P., de, Mouazen, A.M., 2020a. Effect of X-Ray Tube Configuration on Measurement of Key Soil Fertility Attributes with XRF. *Remote Sens* 12, 963. <https://doi.org/10.3390/rs12060963>.
- Tavares, T.R., Mouazen, A.M., Alves, E.E.N., Dos Santos, F.R., Melquiades, F.L., De Carvalho, H.W.P., Molin, J.P., 2020b. Assessing soil key fertility attributes using a portable X-ray fluorescence: A simple method to overcome matrix effect. *Agronomy* 10. <https://doi.org/10.3390/agronomy10060787>.
- Van Raij, B., Andrade, J.C., Cantarella, H., Quaggio, J.A., 2001. *Análise química para avaliação de solos tropicais*. IAC, Campinas, Brazil.
- Weindorf, D.C., Chakraborty, S., 2016. Portable X-ray Fluorescence Spectrometry Analysis of Soils. *Methods Soil Anal.* 1, 1384–1392. <https://doi.org/10.2136/methods-soil.2015.0033>.
- Weindorf, D.C., Zhu, Y., McDaniel, P., Valerio, M., Lynn, L., Michaelson, G., Clark, M., Ping, C.L., 2012. Characterizing soils via portable x-ray fluorescence spectrometer: 2. Spodic and Albic horizons. *Geoderma* 189–190, 268–277. <https://doi.org/10.1016/j.geoderma.2012.06.034>.
- Weindorf, D.C., Paulette, L., Man, T., 2013. In-situ assessment of metal contamination via portable X-ray fluorescence spectroscopy: Zlatna, Romania. *Environ. Pollut.* 182, 92–100. <https://doi.org/10.1016/j.envpol.2013.07.008>.
- Wolksa, J., 2005. Safeguarding the environment - XRF analysis of heavy metals in polyethylene. *Plast. Addit. Compd.* 7, 36–39. [https://doi.org/10.1016/S1464-391X\(05\)00334-X](https://doi.org/10.1016/S1464-391X(05)00334-X).
- Xu, D., Zhao, R., Li, S., Chen, S., Jiang, Q., Zhou, L., Shi, Z., 2019. Multi-sensor fusion for the determination of several soil properties in the Yangtze River Delta, China. *Eur. J. Soil Sci.* 70, 162–173. <https://doi.org/10.1111/ejss.12729>.